

Supramolecular Porous Organic Nanocomposites for Heterogeneous Photocatalysis of a Sulfur Mustard Simulant

Yassine Beldjoudi, Ahmet Atilgan, Jacob A. Weber, Indranil Roy, Ryan M. Young, Jierui Yu, Pravas Deria, Alan E. Enciso, Michael R. Wasielewski, Joseph T. Hupp,* and J. Fraser Stoddart*

Efficient heterogeneous photosensitizing materials require both large accessible surface areas and excitons of suitable energies and with well-defined spin structures. Confinement of the tetracationic cyclophane (ExBox⁴⁺) within a nonporous anionic polystyrene sulfonate (PSS) matrix leads to a surface area increase of up to 225 m² g⁻¹ in ExBox•PSS. Efficient intersystem crossing is achieved by combining the spin-orbit coupling associated to Br heavy atoms in 1,3,5,8-tetrabromopyrene (TBP), and the photoinduced electron transfer in a TBP◊ExBox⁴⁺ supramolecular dyad. The TBP◊ExBox⁴⁺ complex displays a charge transfer band at 450 nm and an exciplex emission at 520 nm, indicating the formation of new mixed-electronic states. The lowest triplet state (T₁, 1.89 eV) is localized on the TBP and is close in energy with the charge separated state (CT, 2.14 eV). The homogeneous and heterogeneous photocatalytic activities of the TBP◊ExBox⁴⁺, for the elimination of a sulfur mustard simulant, has proved to be significantly more efficient than TBP and ExBox⁴⁺, confirming the importance of the newly formed excited-state manifold in TBP◊ExBox⁴⁺ for the population of the low-lying T₁ state. The high stability, facile preparation, and high performance of the TBP◊ExBox•PSS nanocomposites augur well for the future development of new supramolecular heterogeneous photosensitizers using host–guest chemistry.

transformation is by using heavy atoms since spin-orbit (λ) coupling increases proportionally with the increase in the atomic number ($\lambda \propto Z^4$). The lone-pair electrons of heavy atoms additionally augment intersystem crossing (ISC) as evident by the El-Sayed rule^[6] which states that $^1S(\pi, \pi^*) \rightarrow ^3T(n, \pi^*)$ ISCs are faster than $^1S(\pi, \pi^*) \rightarrow ^3T(\pi, \pi^*)$ transitions, and $^1S(n, \pi^*) \rightarrow ^3T(\pi, \pi^*)$ are faster than $^1S(n, \pi^*) \rightarrow ^3T(n, \pi^*)$ transitions. To a lesser extent, intramolecular charge transfer (ICT) in donor–acceptor (D–A) dyads has been employed in the design of heavy atoms-free photosensitizers. For instance, it has been reported^[7] that the utilization of an intramolecular D–A boron-dipyrromethene–anthracene (BODIPY–anthracene) dyad which undergoes a charge separation between the two units, acts as an efficient triplet sensitizer on account of the very small S–T gap (ΔE_{ST}). More recently, other investigations have led to the report^[8] that charge-transfer (CT) states formed in the BODIPY–Pyrene D–A dyad, as a

In recent years, triplet excited-state chromophores have attracted considerable attention on account of their applications in photodynamic therapy,^[1] optoelectronic devices,^[2] photocatalysis,^[3] bioimaging and sensing,^[4] and photon up-conversion.^[5] The most common strategy to enhance the singlet-triplet (S–T)

result of photoinduced electron transfer recombine to yield the BODIPY triplet excited state. In the presence of molecular oxygen, BODIPY–Pyrene dyads sensitize singlet oxygen (1O_2) with quantum yields of up to 0.75. In this context, the design of an efficient photosensitizer requires an understanding of

Dr. Y. Beldjoudi, A. Atilgan, Dr. J. A. Weber, Dr. I. Roy, Dr. R. M. Young, Dr. A. E. Enciso, Prof. M. R. Wasielewski, Prof. J. T. Hupp, Prof. J. F. Stoddart
Department of Chemistry
Northwestern University
Evanston, IL 60208, USA
E-mail: j-hupp@northwestern.edu; stoddart@northwestern.edu

Dr. R. M. Young, Prof. M. R. Wasielewski
Institute for Sustainability and Energy
Northwestern University
Evanston, IL 60208, USA

 The ORCID identification number(s) for the author(s) of this article can be found under <https://doi.org/10.1002/adma.202001592>.

J. Yu, Prof. P. Deria
Department of Chemistry and Biochemistry
Southern Illinois University
1245 Lincoln Drive, Carbondale IL 62901, USA

Prof. J. F. Stoddart
Institute for Molecular Design and Synthesis
Tianjin University
92 Weijin Road, Nankai District, Tianjin 300072, China

Prof. J. F. Stoddart
School of Chemistry
University of New South Wales
Sydney, NSW 2052, Australia

DOI: 10.1002/adma.202001592

the different parameters which promote exciton transformation. Theoretical investigations^[9] of the S–T transformation have shown that, besides the well-recognized importance of the ΔE_{ST} and heteroatom participation for exciton transformation, the two excited states should contain the same components of the transition configurations to establish the transformation channels in bridging the spin-forbidden transitions between two electronic states with different spin multiplicities. Hence, without the matching energy gap, the excitons are weak in S–T transformation because of the lack of enough energy from thermal vibrations or other suitable ways in dissipating excess energy.

In the past decade, considerable interest has been devoted toward the photo-oxidation of the sulfur mustard (SM) and 2-chloroethyl ethyl sulfide (CEES) using 1O_2 since the latter is a mild oxidant and photocatalysis has been proven to involve faster kinetics and to be more selective with the less harmful sulfoxide derivative, 2-chloroethyl ethyl sulfoxide (CEESO), is formed as a major product while the 2-chloroethyl ethyl sulfone derivative (CEESO₂), is a minor product.^[10] Several porous materials, such as metal-organic frameworks (MOFs) and covalent organic frameworks (COFs), with photosensitizing properties^[11] have been utilized for heterogeneous photocatalysis of SM or CEES since the large surface areas of these porous materials facilitate accessibility of the reactants to the photoactive sites. Processability of these crystalline powder materials for use in military protective equipment (MPE), however, remains challenging. Recently, Karwacki and co-workers^[12] reported efficient photocatalysis of CEES to CEESO using 4,4-difluoro-4-bora-3a,4a-diaza-s-indacene (BODIPY) photosensitizers doped into organic polymeric matrices. Nevertheless, the weak interactions through dispersive forces of the BODIPY photosensitizers to the polymer matrices hamper development of viable MPEs because of the leaching of the photosensitizer under catalytic conditions. In addition, a large amount of photocatalyst is required to decrease the conversion lifetime to <1 min. In this context, development of sustainable photosensitizing organic materials for the heterogeneous catalysis of SM or CEES requires that the material fulfill four main requirements: (i) the material is porous, increasing the photoactive surface area and facilitating the diffusion of reactant and products, (ii) 1O_2 generation is efficient, (iii) the material is stable under photocatalytic conditions, and (iv) its preparation is easy, inexpensive, scalable, and capable of being incorporated into MPEs.

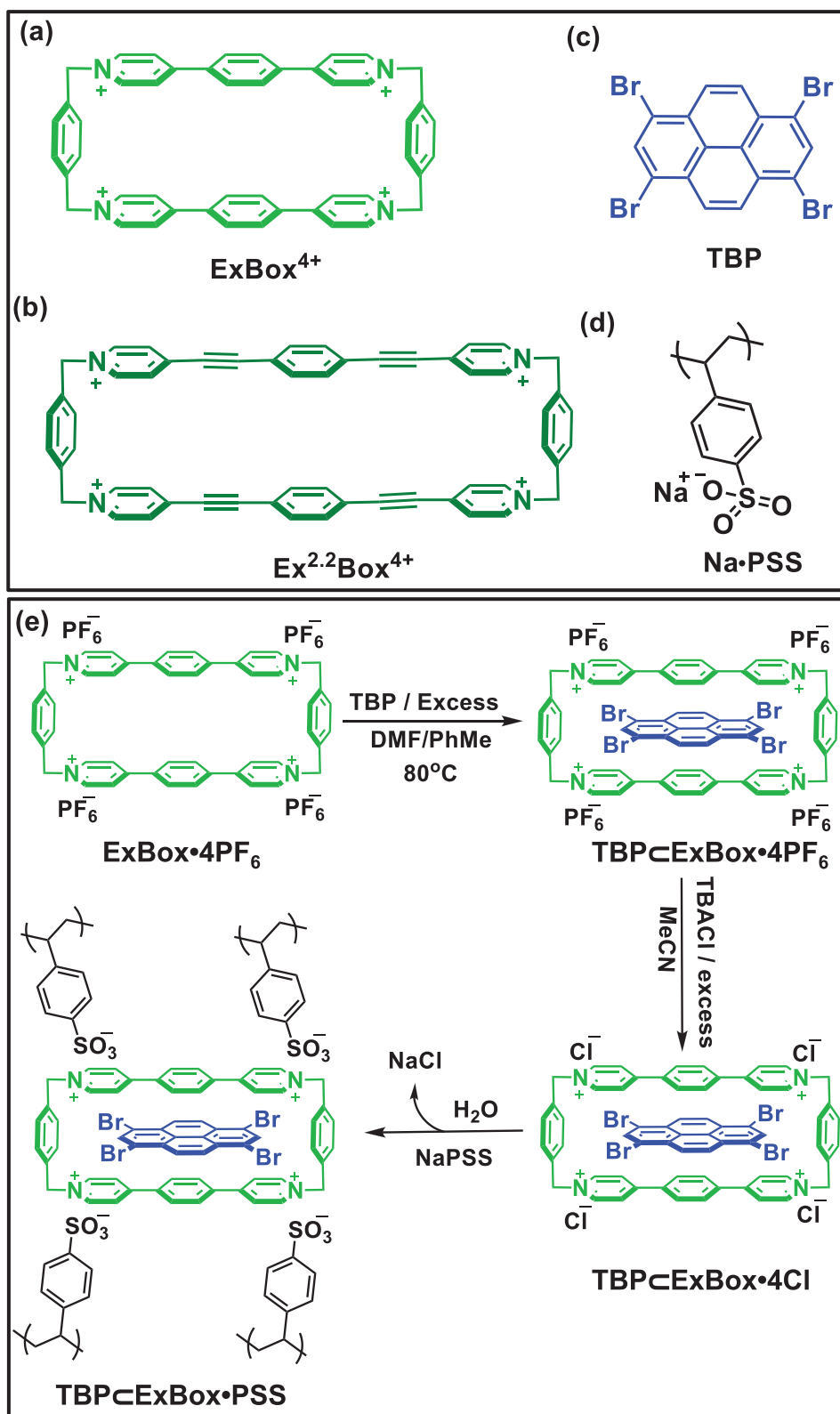
In the present article, we describe (Scheme 1) the preparation of supramolecular porous organic composites using an anionic polymeric matrix such as Polystyrene Sodium Sulfonate (Na•PSS) and extended tetracationic cyclophanes such as ExBox⁴⁺ and Ex^{2,2}Box⁴⁺. The rigidly defined cavities of these cyclophanes, when assembled within a polymeric matrix relying on electrostatic interactions, offers porous properties that are necessary in order to optimize the diffusion of reactants and products within them and increase the active surface area for 1O_2 generation. Furthermore, tetracationic cyclophanes such as ExBox⁴⁺ are attractive candidates for ultrafast intermolecular CT from an electron-rich guest,^[13] intramolecular through-bond CT from the *p*-xylylene bridges to the extended bipyridinium units^[14] and multielectron accumulation,^[15] leading to an array^[16] of accessible mixed-valence states, and

energy transfer from ExBox⁴⁺. Other investigations reported^[17] that the close interaction and the significant orbital overlap between the PDI (perylene diimide) as a guest and ExBox⁴⁺ acting as a host, enables ultrafast energy transfer to proceed by the electron exchange Dexter mechanism.^[18] In addition, incorporation of heavy atoms into the cyclophane leads to an efficient quenching of the fluorescence as a result of efficient spin-orbit ISC pathways leading to the generation of the triplet state of the PDI guest.^[16]

Here, we propose to utilize 1,3,6,8-tetrabromopyrene (TBP) as an electron donor with ExBox⁴⁺ as the electron acceptor in order to form a host–guest D–A supramolecular complex, namely, TBP⊂ExBox⁴⁺. This complex is expected (Figure 1) to promote the S–T exciton transformation between the excited states of the two components, enhancing ISC to populate the low-lying locally excited (LE) triplet state (T_1) of TBP. This design strategy requires (i) efficient CT between the guest (D) and host (A), (ii) the two fluorophores absorb similar radiation wavelengths in order to access the excited-states of both chromophores, (iii) a small ΔE_{ST} (<0.37 eV) and small distance (≈ 3.5 Å) between the D and A in order to facilitate spin-orbit charge-transfer intersystem crossing^[19] (SOCT-ISC), (iv) the energies of both the CT and LE T_1 states must be similar, and (v) incorporation of heteroatoms (N atoms) in the host (ExBox⁴⁺) and the guest (Br atoms) which can, not only facilitate the S–T transformation, but also offer a low lying triplet state that can promote energy transfer to molecular oxygen^[20] ($^1\Sigma = 1.63$ eV).

From a practical perspective, the very low solubility of the TBP in organic and aqueous media at ambient temperatures is necessary in order to enhance the stability of the supramolecular photocatalyst since host–guest formation is not in equilibrium. It was previously reported^[21] that water-soluble cobalt(III) tetrahedral coordination capsules exhibit non-equilibrium guest binding properties because of the hydrophobic effect which is associated with the low solubility of the guest molecules in aqueous media. Finally, incorporation of the tetracationic TBP⊂ExBox⁴⁺ photosensitizer within the anionic matrix of PSS leads to the formation of a stable and porous composite for the heterogeneous photocatalysis of CEES. All compounds have been characterized in solution and in the solid state by absorption, diffuse reflectance and fluorescence spectroscopies. Furthermore, the electronic properties of the host–guest complex have been unraveled using transient absorption spectroscopy and time-dependent DFT calculations. Finally, we have investigated the photocatalytic performance of TBP⊂ExBox⁴⁺•4Cl, and TBP⊂ExBox⁴⁺•PSS for the elimination of the sulfur mustard simulant (CEES) in both homogeneous and heterogeneous liquid-phase reactions.

The ExBox•4PF₆ and Ex^{2,2}Box•4PF₆ cyclophanes were synthesized following protocols already reported in the literature.^[22] Although TBP is insoluble in the most common organic solvents, at high temperatures it becomes soluble in PhMe to afford a pale-yellow solution. The host–guest complex TBP⊂ExBox•4PF₆ can be formed (Scheme 1e) by dropwise addition of TBP, solubilized in hot PhMe into a solution of ExBox•4PF₆ in hot dimethyl formamide (DMF). After heating the mixture for 24 h at 80 °C, an intense yellow/orange colored solution is formed. After evaporation of the solvent and solubilization of TBP⊂ExBox•4PF₆ in MeCN, the



Scheme 1. (top) The structural formulas of building blocks utilized in the design of supramolecular photosensitizing porous nanocomposites for heterogeneous photocatalysis. a) ExBox⁴⁺, b) Ex^{2.2}Box⁴⁺, c) 1,3,6,8-tetrabromopyrene (TBP), d) Sodium Polystyrene Sulfonate (Na•PSS), e) Synthesis of the TBPcExBox•4PF₆, TBPcExBox•4Cl, and TBPcExBox•PSS composites.

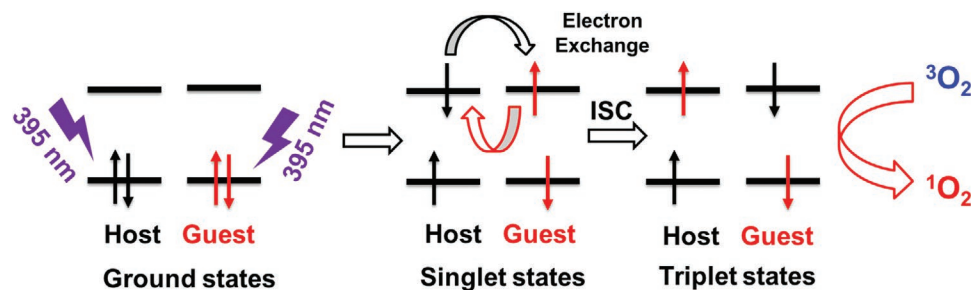


Figure 1. The photoinduced electron exchange in a D–A dyad, acting as an efficient triplet photosensitizer.

insoluble excess of TBP can be removed by filtration. Tetrabutylammonium chloride was added to the MeCN solution containing TBP◊ExBox•4PF₆ in order to exchange the PF₆[−] to Cl[−] anions, a process that renders the cyclophanes soluble in aqueous media. After isolation of the TBP◊ExBox•4Cl complex as a yellow powder, it was dissolved in H₂O and Na•PSS was added dropwise under strong agitation to form (Scheme 1e) a precipitate of TBP◊ExBox•PSS composite of 5/3 w/w ratio. The cyclophane has four positive charges and requires four styrene sulfonate (C₈H₇O₃S[−]) anions in order to calibrate the charges leading to the dispersion of the TBP◊ExBox⁴⁺ along the polymer backbone. The very low solubility of the TBP, combined with the trapping of TBP◊ExBox⁴⁺ within the PSS polymer matrix as a result of electrostatic interactions, is essential in order to enhance the stability of the composite in both aqueous and organic media for efficient heterogeneous photocatalysis.

In order to ascertain the role of the host–guest D–A complex in photocatalysis, the ExBox•PSS and Ex^{2.2}Box•PSS composites have also been prepared (Schemes S1 and S2, Supporting Information) quantitatively following similar protocols. After dissolution of ExBox•4Cl and Ex^{2.2}Box•4Cl in H₂O, Na•PSS was added dropwise to form the ExBox•PSS and Ex^{2.2}Box•PSS composites at 1/1 and 3/2 w/w ratios, respectively. These composites are insoluble in both aqueous and non-aqueous media. In order to study the optical properties of the composites in aqueous solution, we prepared the two composites at 1/3 and 1/1 w/w ratios, respectively. See the Supporting Information for more details.

The CO₂ adsorption on the ExBox•PSS and Ex^{2.2}Box•PSS composites has been performed (Figure 2a) and compared to the adsorption isotherm of pristine Na•PSS in order to confirm the role of the tetracationic cyclophanes in forming the porous nature of these composites. Figure 2a shows, as expected, a negligible adsorption of CO₂ into Na•PSS at 195 K indicative of its nonporous nature. The rapid increase in CO₂ uptake at low pressures for both ExBox•PSS and Ex^{2.2}Box•PSS indicates the presence of micropores, whilst the continuous increase of the uptake confirms the presence of larger pores. The pore volume plot revealed (Figure S6, Supporting Information) the existence of several pores of different sizes, e.g., medium-sized micropores (7–9 Å) and ultra-micropores (<7 Å). These pore sizes are like those of other porous materials, such as MIL-47 and TIF-1 which possess^[23] pore sizes in a range of 7–9 Å, while the MFI and MOR have pore sizes of <7 Å. Other polymers of intrinsic microporosity (PIMs) have been reported in the literature and exhibit similar pore

sizes.^[24] The Brunauer–Emmett–Teller (BET) surface areas of ExBox•PSS and Ex^{2.2}Box•PSS at 195 K were found (Figure 2a) to be 226 and 86 m² g^{−1} respectively. Clearly, the inherent cavities in the tetracationic cyclophanes, combined with their distribution within an anionic polymeric matrix, leads to an increase in the surface area of the PSS matrix. The differences in the porosity between ExBox•PSS and Ex^{2.2}Box•PSS, however, can be attributed to the coexistence of intrinsic porosity associated with the cyclophane’s cavity and the extrinsic porosity associated with the morphology of the composite. It has been

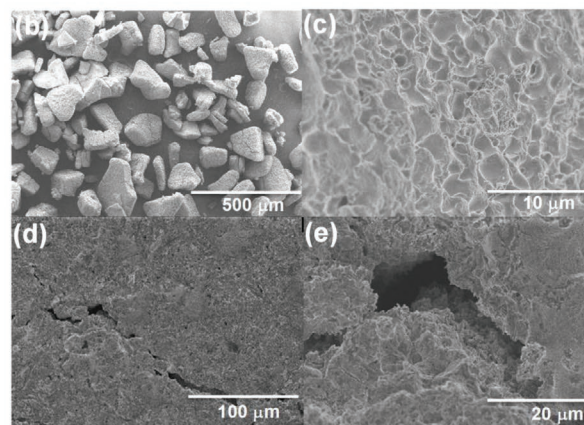
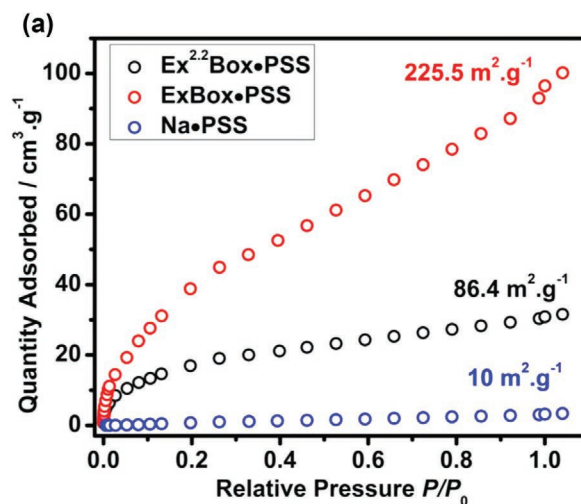


Figure 2. (a) CO₂ sorption isotherms at 195 K for Na•PSS, ExBox•PSS, and Ex^{2.2}Box•PSS. SEM image showing the rough texture of the (b,c) ExBox•PSS composite and (d,e) TBP◊ExBox•PSS composite.

suggested^[24] that microporous materials can be derived directly from soluble polymers whose randomly contorted shapes prevent an efficient packing of the macromolecules in the solid state.

In order to test the diffusion of larger molecules, we investigated the adsorption of tetrathiafulvalene (TTF) inside the ExBox•PSS composite. Previous studies have revealed^[25] that TTF has a relatively strong affinity for the tetracationic cyclophanes, forming dark green host–guest complexes. Addition of ExBox•PSS composite to a solution of the TTF of concentration of 10^{-5} M led to the absorption of the TTF molecules, affording (Figure S10, Supporting Information) a dark green composite as a result of the CT interactions between TTF and ExBox⁴⁺ in the TTF⊂ExBox⁴⁺ host–guest complex. The crystal structure of TTF⊂ExBox⁴⁺ shows (Figure S72, Supporting Information) one molecule of TTF trapped inside the cavity of ExBox⁴⁺, while additional TTF molecules remain outside the cavity. Similarly, in the ExBox•PSS matrix, some TTF molecules are hosted inside the ExBox⁴⁺ cavities, while other TTF molecules reside outside. We conclude that the composite possesses large pores which allow diffusion of both the reactants (CEES, O₂) and product (CEESO) molecules for photocatalytic applications. In recent years, considerable interest has been focused^[26] toward the use of porous materials for catalytic applications on account of their high active surface areas and low diffusion barriers. Scanning electron microscopy (SEM) has revealed that, while the Na•PSS (Figure S7, Supporting Information) has a smooth texture, the composites ExBox•PSS, Ex^{2,2}Box•PSS and TBP⊂ExBox•PSS are all characterized (Figure 2 (bottom), Figures S8 and S9, Supporting Information) by having a rough and spongy texture indicative of their porous natures. Powder XRD has revealed (Figures S4 and S5, Supporting Information) that all the composites are amorphous, confirming the distribution of the tetracationic cyclophanes in the PSS matrix and the absence of phase separation between the amorphous Na•PSS and the crystalline cyclophane phase. Notably, the discrepancy in the porosity and the morphology between ExBox•PSS and Ex^{2,2}Box•PSS implies that the two cyclophanes interact with the PSS matrix differently. The length of ExBox⁴⁺ and Ex^{2,2}Box⁴⁺ are 12 and 17 Å, respectively, while their heights are similar. The distance between the styrene sulfonate units in the PSS backbone is ≈3 Å. In this situation, the discrepancy between the morphologies and porosities of the ExBox•PSS and Ex^{2,2}Box•PSS composites could be associated with different distributions of the cyclophanes in relation to the charged units in the PSS polymer.

Absorption and fluorescence investigations were carried out in order to unravel the electronic properties of the host–guest complex (TBP⊂ExBox•PF₆) in solution and the polymer composites in the solid-state. Na•PSS is colorless in H₂O and its UV–vis absorption profile is characterized (Figure S11, Supporting Information) by the existence of two absorption bands at 223 and 252 nm, while fluorescence spectroscopy has shown (Figure S12, Supporting Information) that excitation at 254 nm offers a single emission band at 308 nm. ExBox•4Cl in H₂O displays (Figure S13, Supporting Information) excitation and emission bands at 358 and 383 nm, respectively, arising from the lowest singlet excited state. The Exbox•PSS composite of 1/3 w/w ratio is soluble in H₂O and displays (Figure S14,

Supporting Information) the characteristic absorption features of ExBox⁴⁺ and PSS. The emission of this composite in aqueous solution exhibits a slight bathochromic shift of 47 nm to become (Figure S15, Supporting Information) centered at 430 nm as a consequence of the change in the polarity and viscosity of the medium.^[27] Time-resolved photoluminescence decay was monitored at 430 nm, using 374 nm as the excitation wavelength. The decay curve was fitted (Figure S15, Supporting Information) to the double-exponential function, resulting in a slow component ($\tau_1 = 1.43$ ns) and a fast one ($\tau_2 = 0.47$ ns).^[28] In PhMe, TBP is weakly soluble and the absorption profile of TBP shows (Figure S20 (left), Supporting Information) several absorption bands at 378, 359, 341, and 293 nm characteristic of the $\pi \rightarrow \pi^*$ and $n \rightarrow \pi^*$ transitions. The diffuse reflectance of TBP reveals (Figure 3a) the existence of two maxima at 320 and 380 nm, similar (Figure S20 (right), Supporting Information) to the solution absorption profile. Upon excitation at 380 nm, TBP offers a featured (Figure S18a, Supporting Information) emission band in a range 400–470 nm ($\lambda_{\text{max}} = 439$ nm, $\Phi_{\text{F}} = 1.62\%$) with a Stokes shift (Table S2, Supporting Information) of 0.22 eV. The singlet excited-state lifetime (Table 1) is rather long ($\tau_1 = 0.11$ ns, $\tau_2 = 0.60$ ns, $\tau_3 = 10.27$ ns), which is associated with the excimer emission as the result of the $[\pi \cdots \pi]$ interactions. Whilst at 298 K the excitation band is centered on 377 nm associated with the existence $[\pi \cdots \pi]$ interaction in the ground state, at 77 K, an intense excitation band appears at 315 nm with a smaller broad band in the range of 340–420 nm (Figure S18b, Supporting Information). The incorporation of TBP inside the cavity of ExBox⁴⁺ does not affect significantly the ground-state electronic properties of either component. Indeed, the absorption spectra of TBP⊂ExBox•4Cl and TBP⊂ExBox•4PF₆ are characterized (Figure S20 (right), Supporting Information) by the overlap of the absorption bands of both the host and guest components, with a maximum absorption centered on 320 and 358 nm in MeCN and H₂O, respectively. The diffuse reflectance spectrum of the TBP⊂ExBox•4PF₆ reveals (Figure 3a) the existence of a broad CT band centered on 455 nm. It follows that the TBP⊂ExBox⁴⁺ supramolecular D–A dyads might exhibit a SOCT-ISC in order to enhance the exciton transformation. Previous work indicates^[29] that efficient ISC can be obtained with intramolecular electron D–A dyads, displaying $n-\pi^* \leftrightarrow \pi-\pi^*$ systems because the electron transfer (charge separation or recombination) will result in magnetic torque on the electron spin which will induce a molecular orbital angular momentum change, enhancing ISC. Steady-state fluorescence spectroscopy revealed (Figure 3b and Table 1) the existence of two emission bands centered on 440 and 512 nm at 298 K. The band at 440 nm can be attributed to TBP monomer emission, while the one at 512 nm is considered to be an exciplex emission (¹S_{1CT}) arising from the TBP⊂ExBox⁴⁺ host–guest complex.

The electronic properties of the TBP⊂ExBox•4PF₆ complex have also been investigated with transient absorption spectroscopy. By exciting at either 414 or 450 nm, the kinetics of the charge separation and recombination for TBP⊂ExBox⁴⁺ were obtained. See Figure 3c and Figures S22–S24 (Supporting Information). In addition, excitation at each of these wavelengths allows deconvolution of the roles of the LE and CT states in the overall electronic properties. Indeed, on excitation at 414 nm the LE state TBP can be accessed, while at 450 nm only the lowest

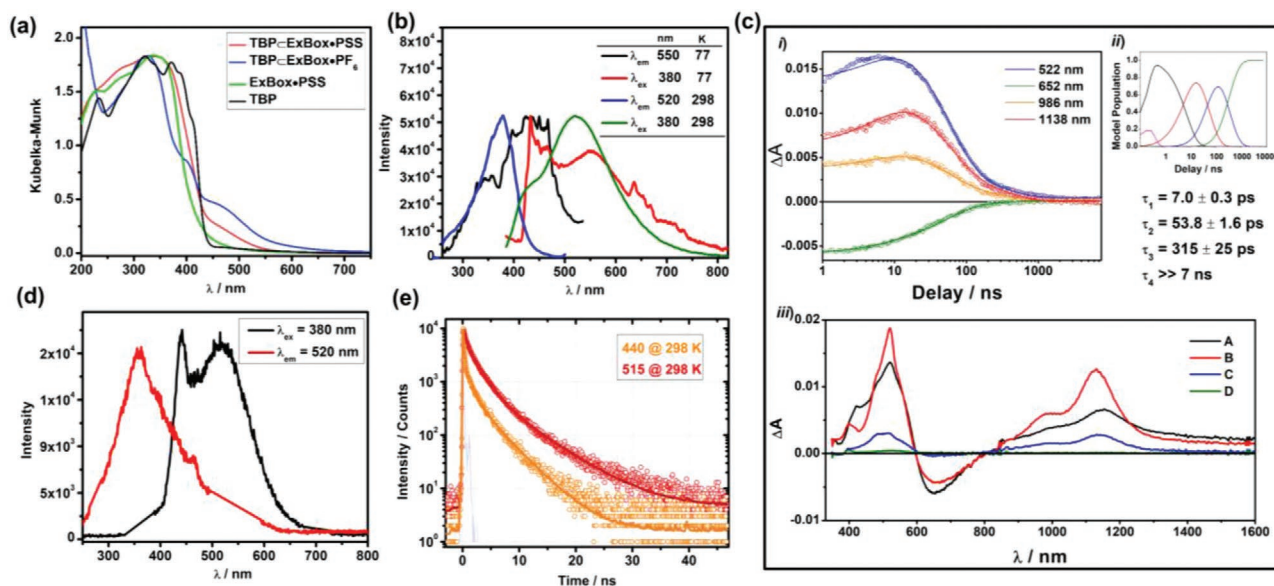


Figure 3. (a) Diffuse reflectance spectra recorded for the TBP-ExBox+PF₆ complex in MeTHF (blue), for the TBP in PhMe (black) and for the ExBox⁴⁺•PSS (green) and TBP-ExBox⁴⁺•PSS composite (red) in the solid state. (b) Excitation and emission spectra of the TBP-ExBox+PF₆ complex in MeTHF, recorded at 77 and 298 K. (c) Kinetic analysis of the femtosecond transient absorption data of TBP-ExBox+PF₆ at $\lambda_{\text{ex}} = 414$ nm showing i) Fits to the solution of a 4-state kinetic model (A \rightarrow B \rightarrow C \rightarrow D). ii) Model populations as a function of time. iii) Evolution-associated spectra for each species in the model. (d) Excitation and emission spectra of the TBP-ExBox+PSS composite. (e) Emission decay of the TBP-ExBox+PSS composite at $\lambda_{\text{ex}} = 405$ nm fitted using a triple exponential fit.

CT state can be reached. Photoexcitation of TBP-ExBox⁴⁺ at 414 or 450 nm results (Figure 3c and Figure S24, Supporting Information) in the appearance of strong peaks at 522, 985, and 1140 nm as well as a radiative recombination band at 655 nm. Similar absorption bands have been observed^[12] for the Perylene-ExBox⁴⁺ CT complex without the radiative recombination band. This radiative recombination gives an estimate of the energy of the CT state of 1.89 eV. The DFT-calculated energy of the lowest triplet (T₁) state is also 1.89 eV, implying that these states may interact via SOCT-ISC. When excited at 414 nm, these bands are formed (Figure 3c and Figure S22, Supporting Information) immediately and rise over the next ≈ 7 ps, then decay in ≈ 54 and ≈ 300 ps. The immediate appearance of the bands associated with ExV⁺ indicates that CT from the LE state of TBP is ultrafast (< 300 fs), as it is the case for Perylene-ExBox⁴⁺. The ≈ 7 ps time constant is associated with a structural relaxation of the charge-separated state,^[13] and the biexponential decay of the TBP⁺-ExBox³⁺ state is most likely a consequence of the distribution of binding geometries in solution. Both recombination processes are slightly longer than the

≈ 40 ps charge recombination observed for Perylene-ExBox⁴⁺. Notably, direct excitation of the CT band ($\lambda_{\text{ex}} = 450$ nm) offers a similar TA profile; however, with generally longer time constants a similar rise occurs (Figure S24, Supporting Information) with ≈ 8.6 ps, then a decay in ≈ 71 ps and a minor-component decay in ≈ 900 ps.

Nanosecond transient absorption measurements leads to the observation (Figure S23, Supporting Information) at $\lambda_{\text{ex}} = 414$ nm of a long-lived triplet of > 1.5 μs , implying that excitation of the upper ¹CT and ¹LE states (S₂, S₃, S₄ states, vide infra) populates the T₁ state of TBP following charge recombination, while excitation of the ¹CT states at 450 nm does not lead to a detectable triplet population. The lack of triplet formation, following 450 nm excitation, is associated with the lower amount of triplet character in the CT state populated by absorption, which is also consistent with the discrepancy in the decay time-constants at different excitation wavelengths. Whilst excitation at 414 nm offers shorter time-constants, associated with the more efficient SOCT-ISC between the upper states (S₂ \rightarrow T₆, S₃ \rightarrow T₆ and S₄ \rightarrow T₈ for example, Figure 5a) with higher triplet character, excitation at 450 nm offers longer time-constants associated with slower SOCT-ISC between the S₁ and T₂ and T₃ states. Thus, the triplet population observed upon higher energy excitation (HLCT states) is a result of a rapid ISC induced by both the heavy Br atoms and SOCT-ISC between the D-A. These results are consistent with the efficient photocatalytic conversion of CEEs at 395 nm, while photoexcitation at 450 nm is very slow (Figure S63, Supporting Information).

Diffuse reflectance measurements on solid films of the ExBox+PSS composite exhibit (Figure 3a) a broad peak in the range of 200–450 nm centered on 350 nm. The ExBox+PSS emission (Figure S16, Supporting Information)

Table 1. Fluorescence parameters of the ExBox+PSS, TBP, and TBP-ExBox+PSS at 298 K.

Sample	λ_{em} [nm]	τ_1 [ns] [Amplitude %]	τ_2 [ns] [Amplitude %]	τ_3 [ns] [Amplitude %]
TBP-ExBox+PSS	440	0.137 [37.97]	1.32 [27.7]	4.031 [34.33]
	515	0.3512 [13.39]	2.027 [56.8]	6.14 [29.81]
ExBox+PSS	480	0.22 [20.27]	1.40 [42.89]	8.23 [36.84]
^{a)} TBP	439	0.11 [40.09]	0.60 [8.55]	10.27 [51.36]

^{a)}In MePh.

is excitation-dependent, ranging from 470 to 525 nm (λ_{ex} 380–450 nm). The emission is centered on 470 nm at $\lambda_{\text{ex}} = 380$ nm (Figure S17, Supporting Information), with a Stokes shift of 0.54 eV (Table S2, Supporting Information) and singlet excited-state lifetimes ($\Phi_{\text{F}} = 1.32\%$, $\tau_1 = 0.22$ ns, $\tau_2 = 1.40$ ns, $\tau_3 = 8.23$ ns at 298 K) (Table 2) slightly larger than those in solution. The TBP◊ExBox⁴⁺•PSS composites show (Figure 3a) an intense broad reflectance peak in the range of 200–440 nm (centered on 360 nm) and a small CT band at 455 nm similar to that of TBP◊ExBox•4PF₆ in solution. The broad absorption spectrum (Figure S21, Supporting Information) extending up to 600 nm indicates the absence of a well-defined band edge in the UV–vis energy range for all the materials. As in the case of TBP◊ExBox•4PF₆ in solution, the composite TBP◊ExBox•PSS displays (Figure 3d) a first emission band at 440 nm and an exciplex emission band at 522 nm ($\lambda_{\text{ex}} = 380$ nm, $\Phi_{\text{F}} = 2.18\%$) with a Stokes shift of 1.07 eV (Tables S1 and S2, Supporting Information), indicating of persistence of the host–guest complex in the composite. The time-correlated emission measurements at $\lambda_{\text{ex}} = 405$ nm revealed the existence of two components with different S_1 lifetimes at 440 nm ($\tau_1 = 0.14$ ns, $\tau_2 = 1.32$ ns, $\tau_3 = 4.03$ ns) and 515 nm ($\tau_1 = 0.35$ ns, $\tau_2 = 2.02$ ns, $\tau_3 = 6.14$ ns)^[30] (Figure 3e and Table 1) which are associated with TBP and TBP◊ExBox⁴⁺, respectively. It is noteworthy that the ¹S_{CT} lifetimes of TBP◊ExBox⁴⁺ in the solid state are slightly shorter than the ¹LE states in the two separate components, TBP and ExBox•PSS, indicating the existence of competing decay pathways. Furthermore, this observation indicates the formation of a new mixed dipole entity in TBP◊ExBox⁴⁺ that exhibits faster relaxation from the CT state, consistent with the TA studies which support efficient ISC associated with the large SOC of the Br atoms but also the influence of SOCT-ISC in the D–A dyad.

In order to understand better the electronic properties of the TBP◊ExBox⁴⁺ complex and obtain an estimation of the singlet-triplet energy gap (ΔE_{ST}), we utilized both the APFD and the B3LYP functionals in conjunction with the 6–31G(d) basis set to calculate molecular geometries. Optimization of the superstructure of the TBP◊ExBox⁴⁺ at the B3LYP/6-31G(d) energy level leads to a larger interplanar distance (≈ 4.2 Å) between the TBP and Exbipy²⁺ units while utilization of the APFD functional resulted in a superstructure (Figure S33, Supporting Information) with interplanar distances between TBP and Exbipy²⁺ of 3.5 Å, similar to those reported^[22] for the crystal structures of polyaromatic compounds inside ExBox⁴⁺. The discrepancy between these optimized superstructures is a result of incorporation of an empirical dispersion correction term within the APFD formalism, while dispersion interactions are neglected within the B3LYP functional.^[31] In addition, these two geometries offer the possibility to determine the energy of the LE states of the TBP and ExBox⁴⁺ and, hence, unravel the role of the orbital overlap between the D–A into the formation of mixed excited states. Satisfied by the presence of zero negative frequencies, gas-phase TD-DFT calculations have been subsequently carried out at the B3LYP/6-31G(d) level of theory using Gaussian16 software.^[32] Here we discuss the electronic properties of TBP◊ExBox⁴⁺ derived from the APFD/6-31G(d) optimized structure (Figure 5 and Table 2), while a detailed analysis of the electronic properties of the B3LYP/6-31G(d) geometry can be found in the Supporting Information. The molecular electrostatic potential difference map (CI–SCF) of the TBP◊ExBox⁴⁺ complex revealed (Figure S42a, Supporting Information) that the negative electron density is localized on TBP, while the positive charge density is localized on ExBox⁴⁺, consistent with the electron D–A nature of the complex. The calculated absorption spectrum (Figure S42b, Supporting Information) reproduces well the experimental

Table 2. Excitation energy (E in eV), oscillator strength (f), transition configuration of $S_0 \rightarrow S_n$ and $S_0 \rightarrow T_n$ for exciton transformation, and energy gap of the singlet-triplet splitting (ΔE_{ST}). These calculation are based on the APFD-6-31G(d) geometry-optimized molecular structure.

S_n	E^a [eV]	Oscillator strength $[f^b]$	Transition configuration [%]	T_n	E [eV]	Transition configuration [%]	ΔE_{ST}	ΔE_{ST} [eV]
1	2.24	0.0004	H→L+1 (99.7%)	1	1.89	H→L+2 (88%), H→L+3 (5.2%)	^{2,1} ΔE_{ST}	1.0971
2	2.99	0.0097	H→L+2 (33.8%), H→L+3 (62.6%)	2	2.19	H→L (99.6%)	^{1,2} ΔE_{ST}	0.049
3	3.11	0.0131	H-1→L+1 (14.1%) H→L+2 (45.3%), H→L+3 (31.1%)	3	2.24	H→L+1 (98.4%)	^{1,3} ΔE_{ST}	0.0076
4	3.20	0.2478	H-1→L+1 (80.5%), H→L+2 (8.8%)	4	2.56	H-4→L+1 (29.8%), H-1→L (47.5%)	^{3,4} ΔE_{ST}	0.5546
5	3.41	0.0017	H-3→L (94.5%)	5	2.57	H-4→L+1 (32.8%), H-1→L (43.9%)	^{3,5} ΔE_{ST}	0.5462
6	3.46	0.0012	H-1→L+2 (28.7%) H→L+5 (37.6%), H→L+7 (13.5%)	6	2.96	H→L+3 (80.2%)	^{3,6} ΔE_{ST}	0.1573
7	3.51	0.0346	H-5→L (87.0%), H-4→L (6.0%)	7	3.10	H→L+4 (97.3%)	^{4,8} ΔE_{ST}	0.0065
8	3.55	0.0052	H-6→L+1 (73.2%), H-4→L (17.3%)	8	3.19	H-9→L+1 (19.2%) H-7→L (29.1%), H-1→L+1 (29.1%)	^{4,9} ΔE_{ST}	0.0064
9	3.57	0.2771	H-6→L+1 (18.5%) H-7→L (30.2%), H-4→L (34.3%)	9	3.19	H-9→L (22.5%) H-7→L+1 (20.7%), H-1→L (12.4%)	^{3,10} ΔE_{ST}	0.098
10	3.65	0.323	H-4→L (28.7%), H-7→L (53.7%), H-9→L+1 (5.9%)	10	3.21	H-1→L+2 (10.6%), H→L+3 (10.4%) H→L+5 (38.8%), H→L+7 (17.8%)		

^{a)}H and L represent, respectively, HOMOs and LUMOs; ^{b)}The most similar and energetically close ΔE_{ST} are highlighted with the same color.

Table 3. Homogeneous photocatalysis parameters using 1 mol% of photocatalyst at 395-nm photoirradiation in CD₃OD.

Catalyst	Irradiation time [min]	Total conversion [%]	Full conversion time [min]	$t_{1/2}$ [min]	(CEESO) Selectivity
ExBox ⁴⁺ Cl	20	100	16	7	97
Ex ^{2,2} Box ⁴⁺ Cl	120	60	/	79	34
TBP⊂ExBox ⁴⁺ Cl	27	100	9	3.5	97

absorption profile with dominant bands at 420 and 387 nm. As expected, the HOMO is localized on TBP while the LUMO is localized on ExBox⁴⁺ with an ΔE_{H-L} (HOMO-LUMO energy gap) of 2.74 eV (452 nm) (Table S13, Supporting Information).

The singlet and triplet excited states of the TBP⊂ExBox⁴⁺ complex consist of (Figure 5a and Table 3) LE states in the TBP or ExBox⁴⁺ components, CT excited states, and a hybridized locally charge transfer excited state (HLCT) which is a mixed state between the LE and CT states.^[32] The first CT transition (Table 3), which is the $S_0 \rightarrow S_1$ transition (552 nm, $f = 0.0004$), is associated with the HOMO \rightarrow LUMO+1 (99%) transition. The energy of the S_1 state is consistent with the observation of exciplex emission at 520 nm associated with the radiative charge recombination in the D–A dyad. The $S_0 \rightarrow S_2$ transition at 2.99 eV (415 nm, $f = 0.0097$) corresponds to the ¹HLCT state in involving minor ¹LE transitions on the TBP (HOMO \rightarrow LUMO+2, 34%) and a major ¹CT component (HOMO \rightarrow LUMO+3, 63%) (Table 3). These results are consistent with the weak broad absorption band observed experimentally at 455 nm. Figure 5a presents the excited state energy diagram and transition configurations of the singlet (S_n) and triplet (T_n) excited states of TBP⊂ExBox⁴⁺. Previous investigations have revealed^[9] that the S–T transformation is rather facile when the two excited states contain the same components of transition configurations to establish the transformation channels in bridging the spin-forbidden transitions between two electronic states with different spin multiplicities. The $S_0 \rightarrow S_1$ transition possesses a very weak oscillator strength and involves only a CT transition from TBP to ExBox⁴⁺. Notably, the lowest triplet state (T_1 , 1.89 eV) contains two components namely, the TBP \rightarrow TBP (HOMO \rightarrow LUMO+2, 88%) and CT (HOMO \rightarrow LUMO+3, 5%) relaxation processes, which can be considered essentially as a ³LE state. Computed singlet and triplet excited states of only TBP (Figures S31 and S32, Supporting Information) revealed that the T_1 (1.91 eV) state has similar energies as those found for TBP⊂ExBox⁴⁺, and is significantly lower in energy than the S_1 and T_2 states, hampering, therefore, its population either through ISC or internal conversion (IC) excited-state relaxation mechanisms. The $S_0 \rightarrow T_3$ (2.24 eV) transition is identical to the $S_0 \rightarrow S_1$ transition and is associated with a CT transition in the TBP⊂ExBox⁴⁺ host–guest complex. The S–T transformation between the S_1 and T_3 states occurs through the SOCT-ISC (Table 2) since the $\Delta E_{ST}^{13} = 0.0076$ eV ($\ll 0.37$ eV). The extent of the HOMO–LUMO orbital overlap is small (15%), consistent with the interplanar distances between the TBP and Exbipy²⁺ units of ≈ 3.5 Å and similar to van der Waals radii (3.5 Å) between carbon atoms. These distances are similar to those reported^[22] from crystal structures of Pyrene⊂ExBox⁴⁺. It was previously

proposed^[9] that the minimum requirement for realizing exciton transformation is the matching of the energy levels of the two states based on the thermal equilibrium between the singlet and triplet excited states. Although the exciton transformation channel $S_1 \rightarrow T_3$ (¹CT \rightarrow ³CT) has a very small ΔE_{ST} (≈ 0 eV), the weak f of the CT transitions in the TBP⊂ExBox⁴⁺ leads to a low population of the T_1 state as observed by TA experiments, corresponding to (Figure S63, Supporting Information) a weak photosensitizing efficiency at $\lambda_{ex} = 450$ nm.

The photocatalytic performance of the TBP⊂ExBox⁴⁺ D–A dyad is high in the excitation range 380–420 nm ($\lambda_{max} = 395$ nm, 3.13 eV), and so the photocatalytic properties arise from the ¹HLCT states, S_2 , S_3 , and S_4 (band at 387 nm, Figure S42b, Supporting Information). The $S_0 \rightarrow S_2$ (2.99 eV), $S_0 \rightarrow S_3$ (3.11 eV) and $S_0 \rightarrow T_1$ (1.89 eV) transitions are similar (HOMO \rightarrow LUMO+2 and HOMO \rightarrow LUMO+3), and the ΔE_{ST} is very large (> 1 eV), hampering (Figure 5a) efficient ISC between $S_2 \rightarrow T_1$ and $S_3 \rightarrow T_1$ channels. From the TA experiments, the S–T transformation is more efficient when higher energy excited states are accessed. The $S_0 \rightarrow T_6$ transition configuration is similar to that of $S_0 \rightarrow S_2$ and $S_0 \rightarrow S_3$, both containing a high HOMO \rightarrow LUMO+3 component. The $\Delta E_{ST}^{26} = 0.03$ and $\Delta E_{ST}^{36} = 0.15$ eV, respectively) and implies a facile exciton transformation. It is noteworthy that the $S_0 \rightarrow S_4$ state is characterized by a large oscillator strength ($f = 0.24$) and arises (Figure 4 and Table 2) predominantly from the HOMO–1 \rightarrow LUMO+1 transition. From Table 3, showing $S_4 \rightarrow T_8$ and $S_4 \rightarrow T_9$, the ΔE_{ST} is very small and can serve as a potential channel for ISC. Previous investigations have shown that, even in the absence of heavy atoms, CT states can undergo efficient ISC, through either radical-pair intersystem crossing^[34] (RP-ISC) for long-lived charge separated states or recombination, to form local triplet excited states of either the D or A units using SOCT-ISC.^[19] Recently, dyads combining BODIPY as an electron acceptor and pyrene or perylene as electron donor subunits were shown to display^[7] CT states formed as a result of photoinduced electron transfer and were found to yield triplet excited states of BODIPY.

In order to decipher further the contribution of the LE, CT and HLCT states to the overall ISC process in the TBP⊂ExBox⁴⁺ complex, natural transition orbital (NTO) analysis, based on the singular value decomposition of a 1-particle transition density matrix, was performed. The NTO analysis shows a compact representation of the orbital transformation composition for a given transition. The highest occupied natural transition orbital (HONTO) and the lowest unoccupied natural transition orbital (LUNTO) represent the most dominant electronic transition and excitation amplitude obtained by diagonalizing generalized hole- and particle-density matrices and by applying additional terms that represent the correlation effects. The NTOs offer the best possible particle/hole picture of an excited state and allow unravelling of the dominant role of the one electronic transition for the generation of the corresponding excited state from the ground state (S_0).^[35] The HONTOs and LUNTOs of all the hybridized singlet (S_2 , S_3 and S_4) and triplet states (T_6 , T_8 , T_9 , and T_{10}) were investigated. Within the singlet/triplet excited-state pairs that can undergo exciton transformation (Figure 5c) according to the energy gap law ($|\Delta E_{ST}| < 0.37$ eV), very similar HONTO and LUNTO

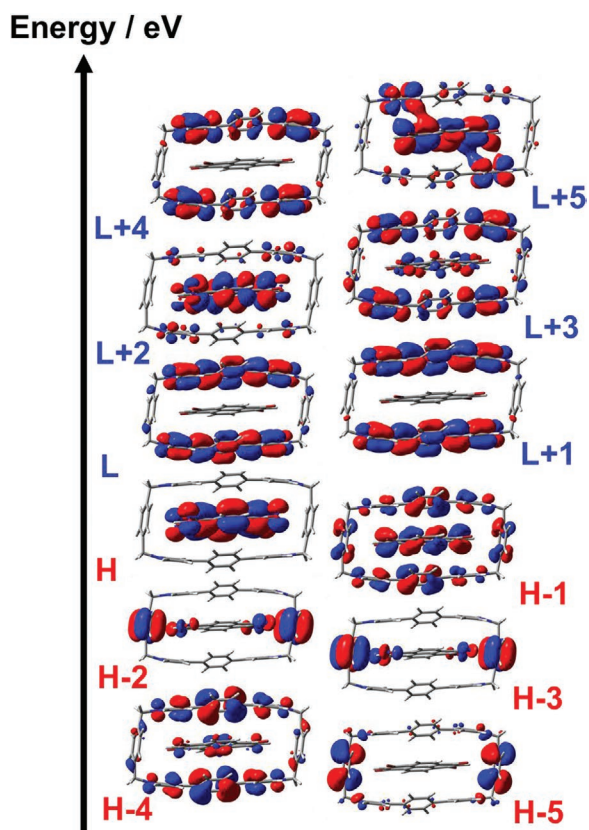


Figure 4. Frontier orbitals of the TBP-ExBox⁴⁺ complex calculated from the APFD/6-31G(d) geometry-optimized molecular structure. H and L represent, respectively, HOMOs and LUMOs.

distributions at both singlet and triplet excited states were observed in TBP-ExBox⁴⁺ where the D dominates HONTO and the A determines LUNTO with very small overlap (I_S and I_T) between HONTO and LUNTO. The almost identical HONTO and LUNTO distributions for $S_0 \rightarrow S_2$ ($I_S = 37\%$) and $S_0 \rightarrow T_6$ ($I_T = 40\%$) transitions, and the small ΔE_{ST} (< 0.37 eV) combined with non-negligible orbital overlap, provide a facile exciton transformation channel for efficient ISC processes between S_2 and T_6 . The NTOs of the S_3 and T_{10} excited states reveal that they have predominantly a LE character associated with the TBP, with a small contribution from the CT states, supporting the role of both the Br atom and CT for in the overall ISC process. The $S_4 \rightarrow T_8$ and $S_4 \rightarrow T_9$ channels are associated with a CT from TBP to the ExBox⁴⁺ with a small contribution from the ExBox⁴⁺ \leftrightarrow ExBox⁴⁺ ISC. At higher excitation energy (> 3.4 eV), CT from the *p*-xylylene unit of the Exbox⁴⁺ is triggered as reported^[13] previously. In this context, utilization of D-A complexes with HLCT character (Figure 5c) can shed important light on the fundamental S-T exciton transformation mechanism in host-guest supramolecular organic complexes, stimulating further the research into purely organic materials capable of facile exciton transformation.

Generation of ¹O₂ by stable microporous organic photocatalysts in both aqueous and organic media provide countless opportunities, not only for the development of environmentally and economically viable materials for the elimination of

SM stockpiles, but also in the design of MPEs. Compared to other oxidants, the reaction of ¹O₂ with CEES leads to the selective formation of less toxic CEESO as a major product, while CEESO₂ is formed as a minor product (Figure 6a) in MeOH solution.^[10] In this study, the photocatalytic activity of the supramolecular photosensitizer TBP-ExBox⁴⁺ has been explored in both homogeneous and heterogeneous media (see the Supporting Information for more details). In order to confirm the role of exciton transformation in the D-A dyad, we also investigated the photocatalytic performances of the TBP, ExBox⁴⁺ and Na•PSS separately in order to unravel the contribution of each component to the overall catalytic activity of the composites. In addition, we explored the photocatalytic activity of the light-sensitive Ex^{2,2}Box⁴⁺ (see the Supporting Information for more details on its optical properties) in order to emphasize the role of incorporating tetracationic cyclophanes into a PSS matrix so as to increase photostability, resulting in enhancement of the photocatalytic selectivity. All the catalytic results are summarized in Tables 3 and 4.

The photocatalysis of CEES with 1% mol catalyst of ExBox•4Cl, Ex^{2,2}Box•4Cl or TBP-ExBox•4Cl relative to the molar charge of CEES was carried out (Figure 6b and Figure S50, Supporting Information) in CD₃OD under photoirradiation at 395 nm (Figure S45, Supporting Information). The kinetics of CEES conversion were monitored by ¹H NMR and decoupled ¹³C NMR. The ExBox•4Cl photocatalyst led (Figure 6b) to 100% conversion of CEES to CEESO after 16 min irradiation. The half-life time of the reaction was observed to be 7 min. The ¹H NMR spectrum (Figure S48, Supporting Information) of CEES contains two triplets centered on 3.7 and 2.9 ppm. After irradiation, these peaks disappear and two multiples appear at 4.0 and 3.3 ppm, corresponding to the chemical shifts of CEESO (Figures S46 and S47, Supporting Information). Formation of this sulfoxide product was also confirmed (Figure S49, Supporting Information) by ¹³C NMR spectroscopy. After 20 min photoirradiation, ¹H NMR spectroscopy shows the formation of 2% CEESO₂ based on the appearance of a peak at 3.57 ppm and negligible amount of vinyl derivatives. X-ray crystallography revealed (Figure S71, Supporting Information) that the molecular structure of ExBox⁴⁺ remained unchanged, indicative of its high stability under the photocatalysis conditions. We tested also the photoactivity of the Ex^{2,2}Box•4Cl as a photosensitizer for the oxidization of CEES; however, we found that only 45% of CEES was converted in 60 min. It is noteworthy that Ex^{2,2}Box•4Cl leads to the formation of different major products, such as CEESO, MeOEES and MeOEESO (Figure 6a and Figures S50 and S51, Supporting Information). Methanol can stabilize sulfide-sulfoxide intermediates^[36] while CEES can undergo methanolysis to form MeOEES if exposed to MeOH for long period of time. The low selectivity (34%) of CEESO formed after 120 min in the presence of (Table 3) Ex^{2,2}Box•4Cl is associated with the decomposition of Ex^{2,2}Box⁴⁺ under photoirradiation as confirmed by UV-vis absorption and ¹H NMR spectroscopies (Figures S29 and S30, Supporting Information). Since TBP is insoluble in MeOH, its photocatalytic performance in homogeneous media could not be obtained. The TBP-ExBox•4Cl D-A dyad is soluble in MeOH and leads to significant increase in the CEES oxidation rate (Figure 6b and Table 3), reaching 100% conversion in less than 10 min

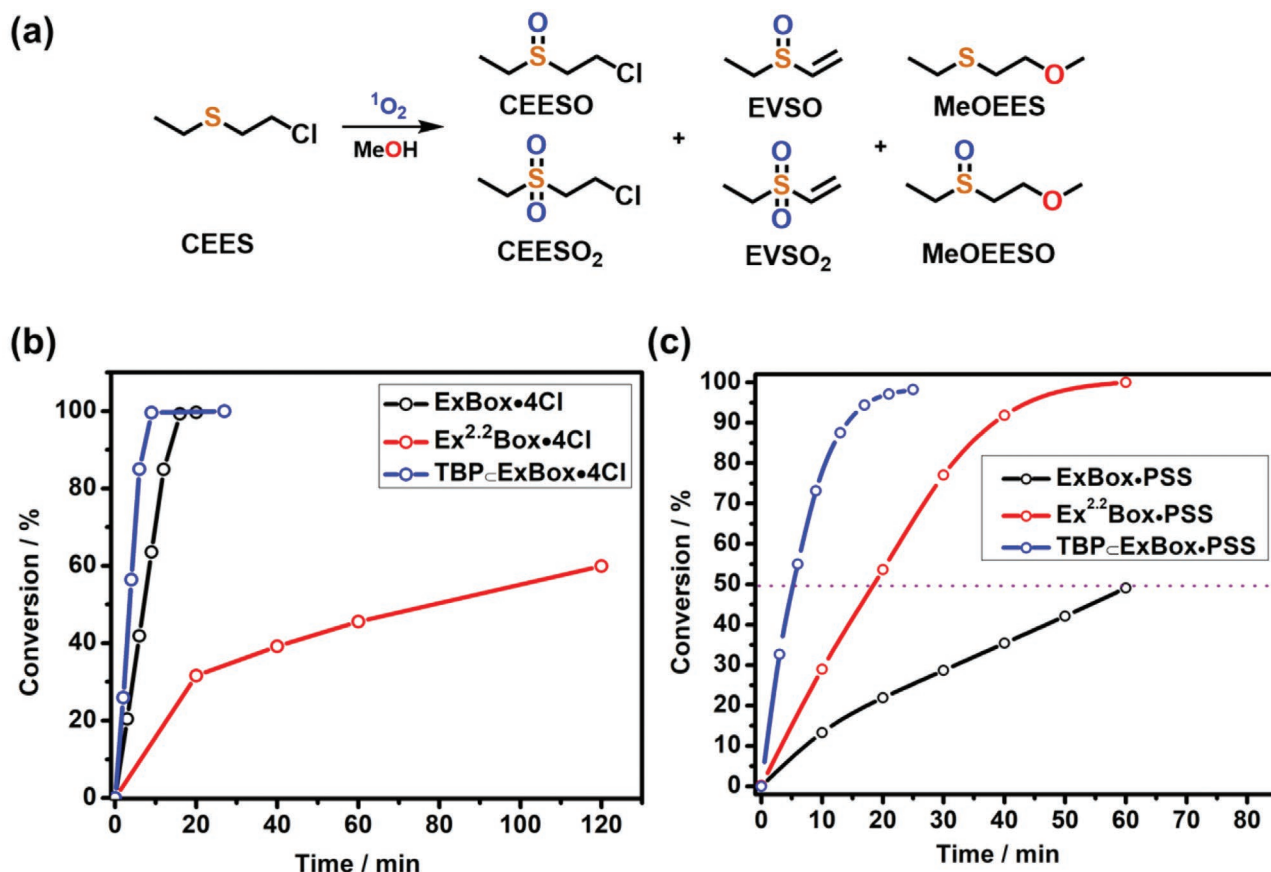


Figure 6. a) Structural formulas of the possible products of the photocatalysis of CEES with $^1\text{O}_2$. b) Homogeneous photocatalysis of CEES in CD₃OD using ExBox⁴⁺•4Cl, Ex^{2.2}Box•4Cl and the TBP_cExBox•4Cl complex. c) Heterogeneous catalysis in liquid phase of CEES with 1% mole ExBox⁴⁺•PSS, Ex^{2.2}Box•PSS and TBP_cExBox•PSS composites.

enhance the transport of reactants ($^3\text{O}_2$, CEES) and products ($^1\text{O}_2$ and CEESO) to and from the photocatalytic sites. Heterogeneous catalysis has been achieved with 1 mol% catalyst of ExBox•PSS, Ex^{2.2}Box•PSS, and TBP_cExBox•PSS relative to the molar charge of CEES, under photoirradiation at 395 nm (Figure 6c). Control reactions have been conducted with PSS and TBP•PSS composites and TBP using identical amounts of catalyst (1 mol%) to estimate the contribution of the PSS and TBP components in the overall photocatalytic performance

Table 4. Heterogeneous photocatalysis parameters using 1 mol% of photocatalyst obtained at 395 nm photoexcitation in MeOH.

Catalyst	Total Photoirradiation time [min]	Total conversion [%]	Time to full conversion [min]	Half-life $t_{1/2}$ [min]	% Selectivity (CEESO)
ExBox•PSS	60	50	/	60	>99
Ex ^{2.2} Box•PSS	60	100	54	18	>99
TBP _c ExBox•PSS	25	100	20	5	>99
TBP•PSS	60	60	/	52	97
TBP	60	50	/	60	58
Na•PSS	60	10	/	/	0

(Figure S57, Supporting Information). All data are summarized in Table 4.

The Na•PSS did not show significant photocatalytic performance except for a slight conversion because of the decomposition of CEES to MeOEES in MeOH (Figure 6a and Figure S69, Supporting Information). The CEES conversion is significantly slower with the ExBox•PSS composite in heterogeneous media (Figure 6c and Table 4) compared to the photocatalytic performance of the ExBox•4Cl in homogeneous media. After 60 min of photoirradiation, the conversion of CEES did not exceed 40%. ¹H and ¹³C NMR spectra revealed (Figures S58 and S59, Supporting Information) the selective formation of CEESO. The slow photoactivity of the ExBox⁴⁺ is consistent with the longer S₁ lifetime (≈ 8 ns) in the solid state than in solution (≈ 1.4 ns), indicating less-efficient ISC in the solid state for ExBox⁴⁺. As in the case of ExBox•PSS, the TBP_cNa•PSS composite showed (Figures S57 and S68, Supporting Information) less than 50% conversion of CEES, implying the low $^1\text{O}_2$ generation. This observation is consistent with DFT calculations which have shown that the T₁ state of TBP cannot be populated efficiently through an ISC or IC mechanism because of the large energy barriers (Figure S32, Supporting Information). Surprisingly, the Ex^{2.2}Box•PSS composite showed a catalytic conversion in heterogeneous media

of 100% in 60 min and $t_{1/2} = 18$ min, whilst in homogeneous media, the conversion did not exceed 45% within a similar photoirradiation timeframe. More importantly, the formation of CEESO was fully selective and ^{13}C NMR spectroscopy did not show (Figure S60, Supporting Information) the appearance of MeOEEs, as observed in homogeneous catalysis as a result of the enhanced stability of the $\text{Ex}^{2,2}\text{Box}^{4+}$ cyclophane within the PSS matrix. Previous investigations^[37] have shown an increase in the stability of air-sensitive S/N radicals when incorporated into polymers matrices. The TBP \subset ExBox \cdot PSS composite has registered a 12-fold increase in the kinetics of conversion of CEES to CEESO compared to ExBox \cdot PSS and TBP \cdot Na \cdot PSS at $\lambda_{\text{ex}} = 395$ nm (Figure 6c and Figure S57, Supporting Information). Within 20 min of photoirradiation, the conversion reached 100% with $t_{1/2} = 5$ min and 100% selectivity for the formation (Table 4) of CEESO. These results are consistent with DFT calculations and spectroscopic investigations showing that excitation of the HLCT excited states triggers an efficient S–T transformation that leads to population of the T_1 state. The energy of the T_1 state (1.89 eV) is close to that of the first excited state of $^1\text{O}_2$ (1.63 eV),^[20] offering (Figure 5b), therefore, an energy gap of ≈ 0.26 eV which is ideal for efficient Dexter energy transfer.^[18,20] Notably, photocatalysis of CEES at $\lambda_{\text{ex}} = 450$ nm (Figures S63 and S64, Supporting Information) is very slow, confirming the weak population of the T_1 states upon excitation of the low-energy ^1CT states. The catalytic performance of TBP \subset ExBox \cdot PSS at 395 nm is comparable (Table S14, Supporting Information) with that of other MOF photocatalysts, such as NU-1000,^[38] UMCM-313^[38] and Al-PMOF-fiber.^[39] Photocatalysis of CEES or SM using porous organic polymers is less common. Recently, a carbazole-based conjugated microporous polymer was reported,^[40] which performs a selective photocatalysis of CEES over a period of 60 min using 8 mole % of the photocatalyst. To the best of our knowledge, the TBP \subset ExBox \cdot PSS composite is among the most efficient organic polymer photocatalysts that has been tested for the elimination of Chemical Warfare Agent simulants. In order to confirm the stability of the TBP \subset ExBox \cdot PSS photocatalyst, we performed a leaching test which consists (Figure S70, Supporting Information) of the removal of the catalyst upon reaching 50% CEES conversion. Further irradiation of the solution showed no significant change in the concentration of CEES, indicating that (i) the TBP \subset ExBox \cdot PSS composite is responsible for the transformation of CEES to CEESO under photoirradiation and (ii) the composite is stable under the photocatalytic conditions because of the absence of a chromophore in solution. Further photoirradiation does not lead to a change in CEES conversion confirming the stability of the supramolecular TBP \subset ExBox \cdot PSS photocatalyst.

In conclusion, supramolecular porous organic composites based on tetracationic cyclophanes (ExBox $^{4+}$ and Ex 2,2 Box $^{4+}$) and an anionic polymer matrix such as polystyrene sulfonate have been prepared. These materials were found to be microporous as evidenced by CO_2 adsorption isotherms. In addition, larger molecules such as TTF can diffuse in/out of the ExBox \cdot PSS composite. While the photocatalysis of CEES by ExBox \cdot 4Cl in solution is fast and selective, in the solid state the conversion of the CEES to CEESO is very slow as a result of stabilization of the

singlet excited state. Other cyclophanes, such as Ex 2,2 Box \cdot 4Cl, are not stable under photoirradiation, and the photocatalysis of CEES is neither fast nor selective. Notably, Ex 2,2 Box \cdot PSS is stable under photoirradiation and the conversion of CEES to CEESO is 100% selective. Although the lowest triplet state (T_1) of 1,3,5,8-tetrabromopyrene is low in energy, it is inaccessible on account of the large energy barrier separating the T_1 states from the S_1 and T_2 states. The efficiency of the singlet to triplet (S–T) transformation in the TBP \subset ExBox $^{4+}$ host–guest complex is associated with a combination of both a large SOC of the Br atoms and SOCT-ISC of the D–A dyad. In addition, DFT calculations revealed the existence of a manifold of excited states in the TBP \subset ExBox $^{4+}$ complex that can enhance the IC relaxation mechanism from the upper triplet states to populate the low-lying T_1 excited state. The efficient S–T transformation and IC relaxation mechanisms play a central role in the enhancement of $^1\text{O}_2$ generation and subsequent increase in photocatalytic performance. The high stability, facile preparation, processability and high performance of the TBP \subset ExBox \cdot PSS composite augur well for the future development of supramolecular heterogeneous photosensitizers using host–guest chemistry. More broadly, these results reveal a number of other opportunities for facile fine-tuning of the S–T transformation in D–A dyads using host–guest chemistry which can unleash fundamental and technological advances for the future design of triplet excited-state chromophores.

Supporting Information

Supporting Information is available from the Wiley Online Library or from the author.

Acknowledgements

Y.B. and A.A. contributed equally to this work. The authors thank Northwestern University (NU) for their generous support of this research. The authors thank the personnel in the Integrated Molecular Structure Education and Research Center (IMSERC) at NU for their assistance in the collection of the data. This project was also supported by the Defense Threat Reduction Agency under grant number HDTRA1-19-1-0010 (J.T.H.). P.D. thanks Southern Illinois University - Carbondale (SIUC) for start up support. It was also supported in the Wasielewski laboratory by the National Science Foundation under grant number DMR-1710104 (M.R.W.).

Conflict of Interest

The authors declare no conflict of interest.

Keywords

cyclophanes, nanocomposites, photocatalysis, photosensitizers, polymers

Received: March 5, 2020

Revised: June 1, 2020

Published online:

- [1] S. B. Brown, E. A. Brown, I. Walker, *Lancet Oncol.* **2004**, *5*, 497.
- [2] R. C. Evans, P. Douglas, C. J. Winscom, *Coord. Chem. Rev.* **2006**, *250*, 2093.
- [3] D. M. Arias-Rotondo, J. K. McCusker, *Chem. Soc. Rev.* **2016**, *45*, 5803.
- [4] X.-D. Wang, O. S. Wolfbeis, *Chem. Soc. Rev.* **2014**, *43*, 3666.
- [5] J. Zhou, Q. Liu, W. Feng, Y. Sun, F. Li, *Chem. Rev.* **2015**, *115*, 395.
- [6] a) M. A. El-Sayed, *J. Chem. Phys.* **1974**, *60*, 4502; b) C. M. Marian, *Wiley Interdiscip. Rev.: Comput. Mol. Sci.* **2012**, *2*, 187.
- [7] M. A. Filatov, S. Karuthedath, P. M. Polestshuk, H. Savoie, K. J. Flanagan, C. Sy, E. Sitte, M. Telitchko, F. Laquai, R. W. Boyle, M. O. Senge, *J. Am. Chem. Soc.* **2017**, *139*, 6282.
- [8] M. A. Filatov, S. Karuthedath, P. M. Polestshuk, S. Callaghan, K. J. Flanagan, T. Wiesner, F. Laquai, M. O. Senge, *ChemPhotoChem* **2018**, *2*, 606.
- [9] R. Chen, Y. Tang, Y. Wan, T. Chen, C. Zheng, Y. Qi, Y. Cheng, W. Huang, *Sci. Rep.* **2017**, *7*, 6225.
- [10] a) Y. Liu, A. J. Howarth, J. T. Hupp, O. K. Farha, *Angew. Chem., Int. Ed.* **2015**, *54*, 9001; b) F. Jensen, A. Greer, E. L. Clennan, *J. Am. Chem. Soc.* **1998**, *120*, 4439.
- [11] a) A. Atilgan, T. Islamoglu, A. J. Howarth, J. T. Hupp, O. K. Farha, *ACS Appl. Mater. Interfaces* **2017**, *9*, 24555; b) H. Wang, G. W. Wagner, A. X. Lu, D. L. Nguyen, J. H. Buchanan, P. M. McNutt, C. J. Karwacki, *ACS Appl. Mater. Interfaces* **2018**, *10*, 18771; c) A. J. Howarth, C. T. Buru, Y. Liu, A. M. Ploskonka, K. J. Hartlieb, M. McEntee, J. J. Mahle, J. H. Buchanan, E. M. Durke, S. S. Al-Juaid, J. F. Stoddart, J. B. DeCoste, J. T. Hupp, O. K. Farha, *Chem. - Eur. J.* **2017**, *23*, 214; d) C. F. Pereira, Y. Liu, A. Howarth, F. Figueira, J. Rocha, J. T. Hupp, O. K. Farha, J. P. C. Tomé, F. A. A. Paz, *ACS Appl. Nano Mater.* **2019**, *2*, 465; e) Y. Liu, C. T. Buru, A. J. Howarth, J. J. Mahle, J. H. Buchanan, J. B. DeCoste, J. T. Hupp, O. K. Farha, *J. Mater. Chem. A* **2016**, *4*, 13809.
- [12] H. Wang, G. W. Wagner, A. X. Lu, D. L. Nguyen, J. H. Buchanan, P. M. McNutt, C. J. Karwacki, *ACS Appl. Mater. Interfaces* **2018**, *10*, 18771.
- [13] a) R. M. Young, S. M. Dyar, J. C. Barnes, M. Juriček, J. F. Stoddart, D. T. Co, M. R. Wasielewski, *J. Phys. Chem. A* **2013**, *117*, 12438; b) I. Roy, S. Bobbala, R. M. Young, Y. Beldjoudi, M. T. Nguyen, M. M. Cetin, J. A. Cooper, S. Allen, O. Anamimoghdam, E. A. Scott, M. R. Wasielewski, J. F. Stoddart, *J. Am. Chem. Soc.* **2019**, *141*, 12296.
- [14] S. M. Dyar, J. C. Barnes, M. Juriček, J. F. Stoddart, D. T. Co, R. M. Young, M. R. Wasielewski, *Angew. Chem., Int. Ed.* **2014**, *53*, 5371.
- [15] R. M. Young, S. C. Jensen, K. Edme, Y. Wu, M. D. Krzyaniak, N. A. Vermeulen, E. J. Dale, J. F. Stoddart, E. A. Weiss, M. R. Wasielewski, D. T. Co, *J. Am. Chem. Soc.* **2016**, *138*, 6163.
- [16] S. T. J. Ryan, J. Del Barrio, I. Ghosh, F. Biedermann, A. I. Lazar, Y. Lan, R. J. Coulston, W. M. Nau, O. A. Scherman, *J. Am. Chem. Soc.* **2014**, *136*, 9053.
- [17] S. T. J. Ryan, R. M. Young, J. J. Henkelis, N. Hafezi, N. A. Vermeulen, A. Hennig, E. J. Dale, Y. Wu, M. D. Krzyaniak, A. Fox, W. M. Nau, M. R. Wasielewski, J. F. Stoddart, O. A. Scherman, *J. Am. Chem. Soc.* **2015**, *137*, 15299.
- [18] D. L. Dexter, *J. Chem. Phys.* **1953**, *21*, 836.
- [19] a) Y. Hou, X. Zhang, K. Chen, D. Liu, Z. Wang, Q. Liu, J. Zhao, A. Barbon, *J. Mater. Chem. C* **2019**, *7*, 12048; b) Z. Wang, M. Ivanov, Y. Gao, L. Bussotti, P. Foggi, H. Zhang, N. Russo, B. Dick, J. Zhao, M. Di Donato, G. Mazzone, L. Luo, M. Fedin, *Chem. Eur. J.* **2020**, *26*, 1091.
- [20] D. Kovalev, M. Fujii, *Adv. Mater.* **2005**, *17*, 2531.
- [21] P. R. Symmers, M. J. Burke, D. P. August, P. I. T. Thomson, G. S. Nichol, M. R. Warren, C. J. Campbell, P. J. Lusby, *Chem. Sci.* **2015**, *6*, 756.
- [22] J. C. Barnes, M. Juriček, N. L. Strutt, M. Frascioni, S. Sampath, M. A. Giesener, P. L. McGrier, C. J. Bruns, C. L. Stern, A. A. Sarjeant, J. F. Stoddart, *J. Am. Chem. Soc.* **2013**, *135*, 183.
- [23] K. C. Kim, T.-U. Yoon, Y.-S. Bae, *Microporous Mesoporous Mater.* **2016**, *224*, 294.
- [24] a) M. M. Khan, G. Bengtson, S. Neumann, M. Rahman, V. Abetz, V. Filiz, *RSC Adv.* **2014**, *4*, 32148; b) P. M. Budd, B. S. Ghanem, S. Makhseed, N. B. McKeown, K. J. Msayiba, C. E. Tattershalla, *Chem. Commun.* **2004**, 230.
- [25] a) M. M. Cetin, Y. Beldjoudi, I. Roy, O. Anamimoghdam, Y.-J. Bae, R. M. Young, M. D. Krzyaniak, C. L. Stern, D. Philp, F. M. Alsubaie, M. R. Wasielewski, J. F. Stoddart, *J. Am. Chem. Soc.* **2019**, *141*, 18727; b) K. Cai, M. C. Lipke, Z. Liu, J. Nelson, T. Cheng, Y. Shi, C. Cheng, D. Shen, J.-M. Han, S. Vemuri, Y. Feng, C. L. Stern, W. A. Goddard III, M. R. Wasielewski, J. F. Stoddart, *Nat. Commun.* **2018**, *9*, 5275.
- [26] a) Y. Luan, N. Zheng, Y. Qi, J. Tang, G. Wang, *Catal. Sci. Technol.* **2014**, *4*, 925; b) W. Zhang, B. Zheng, W. Shi, X. Chen, Z. Xu, S. Li, Y. R. Chi, Y. Yang, J. Lu, W. Huang, F. Huo, *Adv. Mater.* **2018**, *30*, 1800643; c) J. Duan, S. Chen, C. Zhao, *Nat. Commun.* **2017**, *8*, 15341; d) S. Zhao, Y. Wang, J. Dong, C.-T. He, H. Yin, P. An, K. Zhao, X. Zhang, C. Gao, L. Zhang, J. Lv, J. Wang, J. Zhang, A. M. Khattak, N. A. Khan, Z. Wei, J. Zhang, S. Liu, H. Zhao, Z. Tang, *Nat. Energy* **2016**, *1*, 16184.
- [27] a) R. A. Marcus, *J. Chem. Phys.* **1956**, *24*, 966; b) P. Vath, M. B. Zimmt, *J. Phys. Chem. A* **2000**, *104*, 2626; c) J. T. Hupp, Y. Dong, R. L. Blackburn, H. Lu, *J. Phys. Chem.* **1993**, *97*, 3278.
- [28] Y. Wu, J. Zhou, B. T. Phelan, C. M. Mauck, J. F. Stoddart, R. M. Young, M. R. Wasielewski, *J. Am. Chem. Soc.* **2017**, *139*, 14265.
- [29] a) Z. E. X. Dance, S. M. Mickley, T. M. Wilson, A. B. Ricks, A. M. Scott, M. A. Ratner, M. R. Wasielewski, *J. Phys. Chem. A* **2008**, *112*, 4194; b) C. V. Suneesh, K. R. Gopidas, *J. Phys. Chem. C* **2010**, *114*, 18725; c) Y. Dong, A. A. Sukhanov, J. Zhao, A. Elmali, X. Li, B. Dick, A. Karatay, V. K. Voronkova, *J. Phys. Chem. C* **2019**, *123*, 22793.
- [30] J. R. Lakowicz, *Anal. Biochem.* **2001**, *298*, 1.
- [31] A. Austin, G. A. Petersson, M. J. Frisch, F. J. Dobek, G. Scalmani, K. Throssell, *J. Chem. Theory Comput.* **2012**, *8*, 4989.
- [32] M. J. Frisch, G. W. Trucks, H. B. Schlegel, G. E. Scuseria, M. A. Robb, J. R. Cheeseman, G. Scalmani, V. Barone, G. A. Petersson, H. Nakatsuji, X. Li, M. Caricato, A. V. Marenich, J. Bloino, B. G. Janesko, R. Gomperts, B. Mennucci, H. P. Hratchian, J. V. Ortiz, A. F. Izmaylov, J. L. Sonnenberg, W. F. Ding, F. Lipparini, F. Egidi, J. Goings, B. Peng, A. W. Petrone, T. Henderson, D. Ranasinghe, V. G. Zakrzewski, et al., *Gaussian 16 Rev. C.01*, Wallingford, CT **2016**.
- [33] Y. Y. Pan, J. Huang, Z. M. Wang, S. T. Zhang, D. W. Yu, B. Yang, Y. G. Ma, *RSC Adv.* **2016**, *6*, 108404.
- [34] K. Hasharoni, H. Levanon, S. R. Greenfield, D. J. Gosztola, W. A. Svec, M. R. Wasielewski, *J. Am. Chem. Soc.* **1996**, *118*, 10228.
- [35] R. L. Martin, *J. Chem. Phys.* **2003**, *118*, 4775.
- [36] a) J. J. Liang, C. L. Gu, M. L. Kacher, C. S. Foote, *J. Am. Chem. Soc.* **1983**, *105*, 4717; b) R. Limvorapitux, H. Chen, M. L. Mendonca, M. Liu, R. Q. Snurr, S. T. Nguyen, *Catal. Sci. Technol.* **2019**, *9*, 327.
- [37] Y. Beldjoudi, I. Osorio-Román, M. A. Nascimento, J. M. Rawson, *J. Mater. Chem. C* **2017**, *5*, 2794.
- [38] C. T. Buru, Cassandra, T. Buru, M. B. Majewski, A. J. Howarth, R. H. Lavroff, C.-W. Kung, A. W. Peters, S. Goswami, O. K. Farha, *ACS Appl. Mater. Interfaces* **2018**, *10*, 23802.
- [39] D. T. Lee, J. D. Jamir, G. W. Peterson, G. N. Parsons, *Matter* **2020**, *2*, 404.
- [40] Y. Zhi, Z. Yao, W. Jiang, H. Xia, Z. Shi, Y. M. X. Liu, *ACS Appl. Mater. Interfaces* **2019**, *11*, 37578.